Naval Research Laboratory

Washington, DC 20375-5320

NRL/FR/6790--98-9884

A Study of Millimeter-Wave Sintering of Fine-Grained Alumina Compacts

A.W. FLIFLET
R.P. FISCHER

Beam Physics Branch
Plasma Physics Division

R.W. BRUCE

Icarus Research, Inc.
Bethesda, MD

D. LEWIS III
B.A. BENDER
R.J. RAYNE

Mechanics of Materials Branch
Materials Science and Technology Division

L.K. KURIHARA

Potomac Research International
Fairfax, VA

G.-M. CHOW

Physical Metallurgy Branch
Materials Science and Technology Division

October 6, 1998

19981009 064

REPORT DOCUMENTATION PAGE

1. AGENCY USE ONLY (*Leave Blank*)	2. REPORT DATE	3. REPORT TYPE AND DATES COVERED
	October 6, 1998	Interim

4. TITLE AND SUBTITLE

A Study of Millimeter-Wave Sintering of Fine-Grained Alumina Compacts

6. AUTHOR(S)

A.W. Fliflet, R.W. Bruce,* R.P. Fischer, D. Lewis III, L.K. Kurihara,[†] B.A. Bender, G.-M. Chow, and R.J. Rayne

5. FUNDING NUMBERS

TA - EL011-09-41
WU - 5739

TA - MA022-04-41
WU - 3653

7. PERFORMING ORGANIZATION NAME(S) AND ADDRESS(ES)

Naval Research Laboratory
Washington, DC 20375-5320

8. PERFORMING ORGANIZATION REPORT NUMBER

NRL/FR/6790--98-9884

9. SPONSORING/MONITORING AGENCY NAME(S) AND ADDRESS(ES)

Office of Naval Research
800 North Quincy Street
Arlington, VA 22217

10. SPONSORING/MONITORING AGENCY REPORT NUMBER

11. SUPPLEMENTARY NOTES

*Icarus Research, Inc., Bethesda, MD 20814
[†]Potomac Research International, Fairfax, VA 22030

12a. DISTRIBUTION/AVAILABILITY STATEMENT

Approved for public release; distribution is unlimited.

12b. DISTRIBUTION CODE

13. ABSTRACT (*Maximum 200 words*)

A number of high-frequency microwave sintering studies of alumina have reported that sintering proceeds much faster in microwave furnaces when compared to conventional furnaces, and that densification can occur at lower temperatures. These differences have motivated the search for a nonthermal microwave enhancement effect such as the time-averaged microwave field-induced mass transport effect proposed by Rybakov and Semenov. To assess the difference between microwave and conventional sintering and the presence of a nonthermal effect in microwave sintering, a study of millimeter-wave (35 GHz) sintering has been conducted at the Naval Research Laboratory using a well-studied fine-grained (submicron) commercial alumina with reproducibly manufactured properties, Sumitomo AKP-50™. This report describes our results that generally indicate no large differences in the required temperatures for densification of conventionally and microwave-sintered compacts or between the resulting microstructures. The nonthermal microwave effect of Rybakov and Semenov has been estimated for alumina and found to be small.

14. SUBJECT TERMS

Alumina   Microwave
Sintering
Gyrotron

15. NUMBER OF PAGES

23

16. PRICE CODE

17. SECURITY CLASSIFICATION OF REPORT	18. SECURITY CLASSIFICATION OF THIS PAGE	19. SECURITY CLASSIFICATION OF ABSTRACT	20. LIMITATION OF ABSTRACT
UNCLASSIFIED	UNCLASSIFIED	UNCLASSIFIED	UL

CONTENTS

A STUDY OF MILLIMETER-WAVE SINTERING
OF FINE-GRAINED ALUMINA COMPACTS

1. INTRODUCTION

The use of microwaves for heating, sintering/densification, and annealing of ceramic powders and compacts is becoming a well-researched area that is only now gaining some industrial acceptance. Advantages include the ability to deposit energy volumetrically in the sample and the possibility of rapid heating and cooling profiles. Much of the interest in microwave sintering of ceramic compacts derives from the possibilities of much more rapid processing and nonthermal effects, resulting in improved material properties [1]. Most research on ceramic processing by microwaves to date is based on conventional low-frequency (2.45 GHz) microwave applicators [1]. However, such applicators do not couple microwave power efficiently to low-loss ceramics and often have large heating gradients. The recent development of powerful gyrotrons has opened up the millimeter-wave regime ($\geq$ 28 GHz) for processing ceramic materials. Millimeter waves couple more strongly than conventional microwaves to low-absorption ceramics such as pure oxides, increasing the heating efficiency and heating rate and eliminating the need for auxiliary heating at low temperatures. In addition, highly uniform field intensities can be achieved in compact, overmoded cavity applicators.

A number of low- and high-frequency microwave sintering studies have been reported [2]-[11], and the results have generally indicated that sintering proceeds much faster in microwave furnaces when compared to conventional furnaces and that densification can occur at lower temperatures. Lower sintering temperatures are desirable for minimizing grain growth in fine- and ultrafine-grained ceramics. These ceramic materials offer improved fracture toughness and possible superplasticity at elevated temperatures if grain growth during sintering can be controlled. In microwave sintering, thermal energy is deposited in the workpiece by one or more loss mechanisms involving high-frequency oscillations of vacancies or other constituents of the material induced by the microwave field. The significant temperature differences and the processing rate differences observed between conventional and microwave sintering in some studies [2, 9, 10] has motivated the search for a *nonthermal* microwave effect in which the microwave field interacts with the vacancies to produce concentration changes. This type of interaction leads to mass transport rather than the generation of thermal energy. The most promising microwave enhancement model to date has been proposed by Rybakov and Semenov, who showed that time-averaged microwave fields can drive mass transport in ceramics under sintering conditions [12].

One of the difficulties in assessing the presence of a nonthermal effect in microwave sintering has been the wide variation in the published data that is affected by many variables such as grain size, sample preparation, and impurities, as well as difficulties in measuring the conditions in the microwave furnace. For this reason, it was decided to conduct a study of millimeter-wave

(35 GHz) sintering at the Naval Research Laboratory (NRL) using Sumitomo AKP-50^{TM}, a well-studied, fine-grained (submicron) commercial alumina with reproducibly manufactured properties. This material has excellent sintering properties and was used in previous high-frequency microwave sintering studies at Oak Ridge National Laboratory (ORNL) [2], and in a collaboration between Los Alamos National Laboratory (LANL) and Varian (now Communications Power Industries (CPI)) [3]. The ORNL study was conducted using a 28 GHz microwave furnace and showed densification at significantly lower temperatures than in conventional sintering for a 60-min hold time, whereas the LANL/Varian study was conducted with a 60 GHz system and obtained sintering at temperatures typical of conventional sintering but with short (5 min) hold times. This study was undertaken to resolve the differences in these results and to assess the strength and role of the microwave-induced stress proposed by Rybakov and Semenov on the sintering process [12]. It was also of interest to compare the microstructure of 35 GHz microwave-sintered material with that of conventionally sintered alumina because the above-referenced studies addressed only gross densification (pore elimination) during sintering, not details of the microstructure.

The next section outlines the theoretical model proposed by Rybakov and Semenov [12] and estimates the strength of the microwave effect at 35 GHz. Section 3 presents our experimental results, and Section 4 presents the discussion and our conclusions. A derivation of the theoretical results discussed in Section 2 is given in the Appendix.

2.   NONTHERMAL MICROWAVE EFFECT

As is well known, the driving force in conventional sintering is due to the excess surface energy of a system of irregular grains. The surface energy γ, which is ~ 1 Joule/m^2 for ceramics, produces a stress $\sigma^s \approx 2\gamma/R \sim 4$ MPa on a pore of radius $R = 0.5$ μm [13]. This stress leads to a gradient in the vacancy concentration near the grain surface and can drive vacancy-diffusion-based mass transport. It can be shown that the resulting grain deformation rate for densification based on bulk diffusion is given by

$$\dot{\varepsilon} \sim \frac{N_0 D_v \Omega_v}{d^2 k_B T} \sigma^s \tag{1}$$

for volume diffusion, where N_0 is the equilibrium vacancy concentration, D_v is the vacancy diffusion coefficient in the grain volume, Ω_v is the vacancy volume, d is the grain diameter, k_B is the Boltzmann constant, and T is the temperature [14]. A similar expression can be obtained for diffusion along the grain boundary, which is generally the faster process [14].

As pointed out by Freeman et al. [15], in these processes apart from geometrical factors, the grain deformation rate depends on the product of a transport coefficient (the diffusion coefficient) and a driving force (the surface energy stress). Proposed mechanisms for microwave-enhanced sintering generally involve one of the following effects: increased diffusion rate, increased driving force, or anomalously high "internal" temperature. The last effect can usually be ruled out for small samples. Vacancy diffusion proceeds by a jump process in which a vacancy exchanges position with a lattice ion by using thermal energy to overcome a energy barrier. In a system near thermal equilibrium, the diffusion coefficient can be expressed as

$$D_v = D_{v0} \exp(-Q_v/k_B T), \tag{2}$$

where Q_v is the activation energy barrier. In principle, microwaves could affect the diffusion coefficient either by modifying the activation energy or by modifying the vacancy energy distribution.

However, these effects have been found to be small [15, 16]. Recently Rybakov and Semenov showed that the time-averaged interaction between charged vacancies and a microwave field can act as an additional driving force for grain deformation. In this section, their theory is used to obtain an estimate of the microwave driving force expected for sintering of alumina.

Rybakov and Semenov [12] consider the interaction of vacancies with an applied microwave field $\vec{E}(\vec{r}, t) = \vec{E}_0(\vec{r}) \cos(\omega t)$. They use a perturbation approach to calculate the high-frequency and time-averaged components of the vacancy concentration and flux [12]. The Appendix provides derivation of analytical results from their theory, including all of the expressions used in this section. The time-averaged interaction between charged vacancies near the grain boundary and the normal component of the microwave field can be represented as an effective pressure that can be expressed by

$$p = \int_{-\infty}^{0} \frac{q}{\Omega} \left\langle \nu(t) \, \hat{n} \cdot \vec{E}(t) \right\rangle dx, \tag{3}$$

where q is the vacancy charge, $\hat{n} \cdot \vec{E}(t)$ is the normal component of the high-frequency electric field, $\nu(t)$ is the induced high-frequency perturbation in the vacancy concentration, $\langle \; \rangle$ denotes a time average over the wave period, and x is the coordinate normal to the grain boundary. The integrand is nonzero only in a thin region near the grain surface where the concentration perturbation is nonzero. The thickness of this region is characterized by the diffusion scale length $\ell = \sqrt{D_v/\omega}$. Figure 1 shows the geometry of the grain–microwave system.
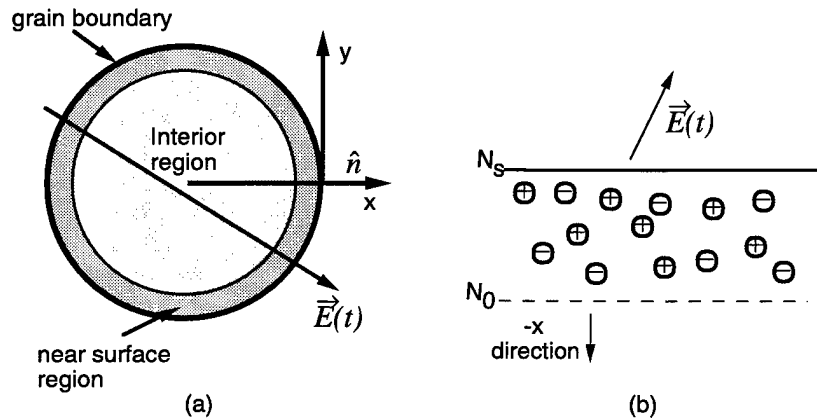

Fig. 1 – (a) Grain and associated microwave field, (b) expanded view of near-surface region

As shown by Rybakov and Semenov, the microwave-induced vacancy pressure is equivalent to an external compressive stress $\sigma^E = p/N_0$. The N_0^{-1} enhancement compared to p is due to the microwave field acting directly on the charged vacancies (atoms neighboring a lattice defect), whereas an external mechanical stress is applied to all of the atoms in the grain, most of which cannot move. By performing the integrations on the right-hand side of Eq. (3) using analytic expressions for the vacancy perturbation and perturbed electric field derived in the Appendix and taking the high-frequency limit, the microwave pressure for a ceramic with two types of oppositely charged but otherwise equivalent vacancies is given by

$$p \approx \frac{N_0^2 q_v^4 D_v^2 \, |E_{ns}|^2}{\varepsilon_0 \varepsilon' \omega^2 \Omega_v^2 k_B^2 T^2}, \tag{4}$$

where E_{ns} is the maximum normal electric field at the grain surface. To obtain an estimate of the microwave-induced pressure, it is convenient to rewrite Eq. (4) in terms of the self-diffusivity,

$D_s = D_v N_0$, of lattice ions, a quantity that can be obtained from tracer experiments

$$p \approx \frac{q_v^4 D_s^2 |E_{ns}|^2}{\varepsilon_0 \varepsilon' \omega^2 \Omega_v^2 k_B^2 T^2}.$$

(5)

Because the vacancy perturbations are limited to the near-surface region of the grain, the self-diffusivity corresponding to grain boundary diffusion at sintering temperatures is assumed (i.e., $D_s \approx 2 \times 10^{-13}$ cm^2/s at 1400°C [17, 18]). The other averaged parameters for oxygen and aluminum vacancies are $q = (2e + 3e)/2 = 4 \times 10^{-19}$ C and $\Omega_v = 1.4 \times 10^{-23}$ cm^3. Assuming a relatively high electric field amplitude of $E_0 = 10$ kV/cm, the microwave field pressure is very small, $p \approx 10^{-11}$ Pa. Even with an enhancement of $N_0^{-1} \approx 10^5$, the effective microwave driving force is about 12 orders of magnitude smaller than the surface energy pressure. Thus it appears that the microwave field pressure is dominated by the surface energy pressure in the sintering of alumina. Note that this estimate has been obtained using a one-dimensional model. In a case where the microwave and surface energy driving forces are comparable, a more realistic model accounting for two-dimensional effects would be needed.

3. SINTERING EXPERIMENTS

Figure 2 shows a schematic of the pulsed 35 GHz gyrotron-powered furnace and diagnostics system. A high pulse repetition frequency (PRF) gyrotron of standard design operates in the TE$_{01}$ circular waveguide mode at a voltage of 70 kV and at currents up to 10 A. It is driven by a hard-tube, variable pulse length (1 to 15 μs) Rockwell Power Systems modulator that has a maximum PRF of 1000 Hz. The gyrotron is placed in the bore of a superconducting magnet, which provides a 13.5-kG field at the gyrotron cavity and an adjustable smaller field at the electron gun cathode. The gyrotron system was originally developed for microwave effects testing at NRL and has been modified for material processing applications. The peak pulsed power of the gyrotron can be varied from 10 to 100 kW, and the maximum duty factor is 0.5%. The gyrotron output efficiency is typically in the range of 20% to 30%, and the average power is controlled by varying the PRF. The maximum average output power is 400 W. The gyrotron output waveguide, which also serves as the electron beam collector, and interaction cavity are water cooled. After exiting an alumina output window, the microwave power passes through a mode converter that transforms the TE$_{01}$ circular waveguide mode into the TE$_{10}$ mode in a rectangular Ka-band waveguide. The power is then transported to the cavity applicator and monitored using standard Ka-band waveguide components pressurized with SF$_6$ or nitrogen to avoid microwave breakdown. The forward and reflected peak powers are sampled using crystal detectors, and the average forward power is also monitored using an Hewlett Packard power meter. The cylindrical, highly overmoded cavity applicator (18-cm diameter, 21-cm height) is isolated from the rest of the waveguide system by a ceramic or mylar window, allowing for a choice of sintering atmospheres. The furnace cavity, shown in Fig. 2, has a 1-cm diameter aperture for injecting the microwave power. A 9.5-mm thick brass plate with an array of 2-mm diameter holes with centers separated by 2.54 mm serves as a viewing port and is covered by a quartz window to allow pressurization of the applicator. Rough measurements of the microwave power distribution using thermal paper showed that the power is strongly peaked along the axis of the cylindrical cavity. Evidence of a standing-wave pattern along the axis was also observed, apparently the result of reflections from the flat end plates of the cavity. The system is operated without a circulator to absorb power reflected from the applicator. The reflected power does not significantly impact the operation of the gyrotron at the present power levels, although switching between closely spaced (~ 100 MHz) modes was occasionally observed. In any case, the reflected

power is quite low at sintering temperatures. Typical measured power reflection coefficients include: $R \sim 0.13$ for the empty cavity, $R \sim 0.05$ when the cavity contains a casket and compact at room temperature, and $R \leq 0.01$ when the compact is hot.
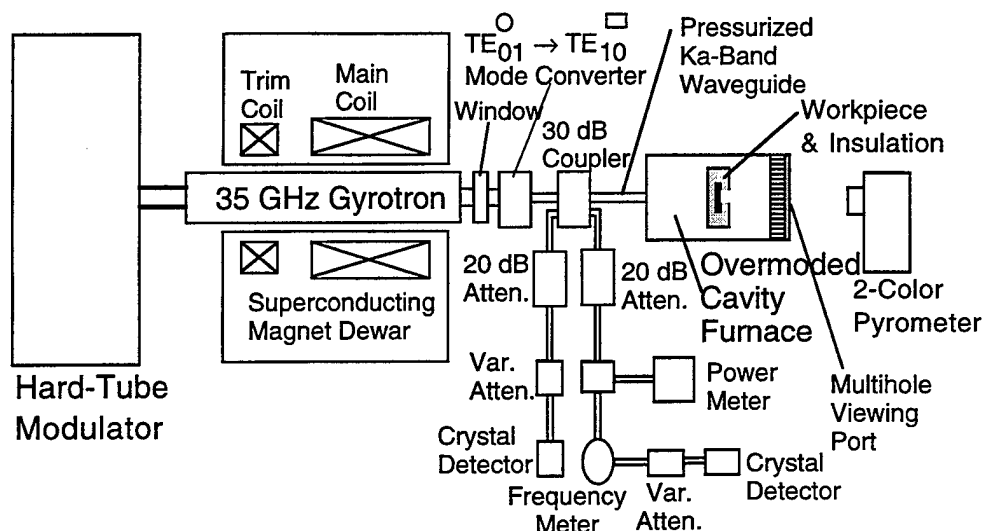
Fig. 2 – Schematic of 35 GHz pulsed gyrotron with multimode resonator furnace

During sintering experiments, the green ceramic compact is placed in a Zircar SALI™ fiber-board casket to provide thermal insulation from the cold-walled cavity, shown schematically in Fig. 3. This type of fiberboard has very little microwave loss. Together with its relatively low density, it resulted in stronger microwave heating of the ceramic compact than of the casket that provides thermal insulation without the complications of hybrid heating. The compact is isolated from the casket by a bed of loose powder, generally the same material as the green compact. The casket has a small hole in the top to allow the surface temperature of the compact to be measured using a Mikron M190 two-color infrared pyrometer.

The microwave sintering process is characterized by several stages: initial heating of the sample at an accelerating rate varying from tens of °C/min to hundreds of °C/min, a variable hold time at the maximum temperature (< 10 min up to 1 h), and rapid cooling of the compact (hundreds of °C/min) following cessation of the microwave power. The accelerating heating rate is associated with the strong dependence of the loss factor with temperature. However, it was possible to control the heating rate by adjusting the microwave power, in our case by varying the PRF. Figure 4 shows a long hold-time heating profile. The figure shows rapid heating of the compact occurring about 14 min after the microwave power was turned on. The fluctuations in the microwave power during the initial heating period are due to the difficulty of maintaining a stable operating point of the experimental gyrotron, which is subject to thermal expansion and load mismatch, particularly during start-up. The figure also shows that small adjustments in the microwave power (obtained by varying the rep-rate) are needed to maintain the compact temperature in the vicinity of 1400°C.

Table 1 summarizes our experimental microwave results, including results for densification, grain growth, and hardness. Hardness data are not available for the short hold-time samples as these
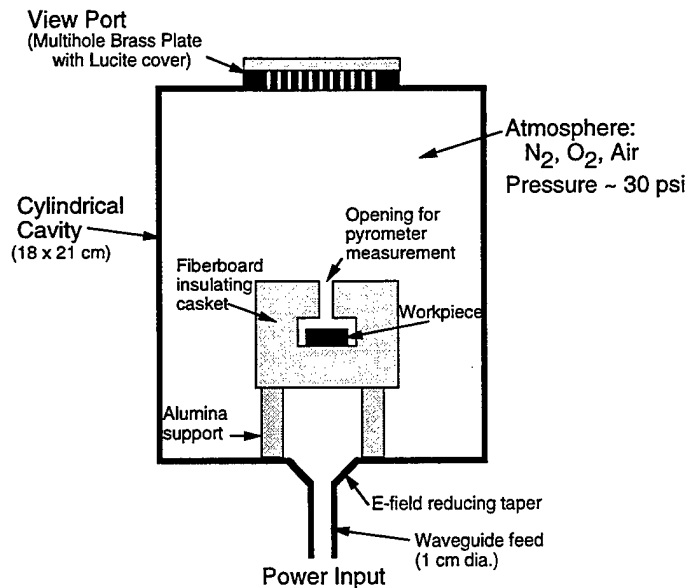
Fig. 3 – Schematic of 35 GHz multimode resonator furnace

were made unusable in the process of microstructure analysis before the hardness tests could be carried out. To explore differences between microwave and conventional sintering, several identically prepared compacts were sintered in a conventional tube furnace. Due to the large thermal mass of the furnace, the heating time was about 1 h and cooling times were 2 h to 3 h. Table 2 shows our data for conventional sintering with a 1-h hold time.

Table 1 – 35 GHz Microwave Sintering Data [Initial Dens. = 57%, Initial Grain Size < 0.1 μm]

Sample	T (°C)	Hold Time (min.)	% RD	Grain Size (μm)	Hardness (GPa)
A	1095	< 10	58	0.18	
B	1200	< 10	70	0.19	
C	1300	< 10	74	0.19	
D	1350	< 10	77	0.22	
E	1400	< 10	85	0.28	
F	1460	< 10	89	0.35	
G	1495	< 10	95	1.00	
H	900	42	59	0.15	1.7
I	1200	60	64	0.20	3.4
J	1400	60	95	3.0	18.5

The relative density (RD) of the sintered compacts were obtained from measurements of the mass and physical dimensions. Our results for microwave and conventionally sintered compacts are shown as a function of peak hold temperature in Fig. 5. This figure also includes the 28 GHz microwave and conventionally sintered data obtained at ORNL [2], and the 60 GHz data obtained by Meek et al. [3] in a collaboration between LANL and Varian (now CPI). In all cases, the compacts were pressed from α-phase Sumitomo AKP-50^{TM} alumina; however, the ORNL compacts contained
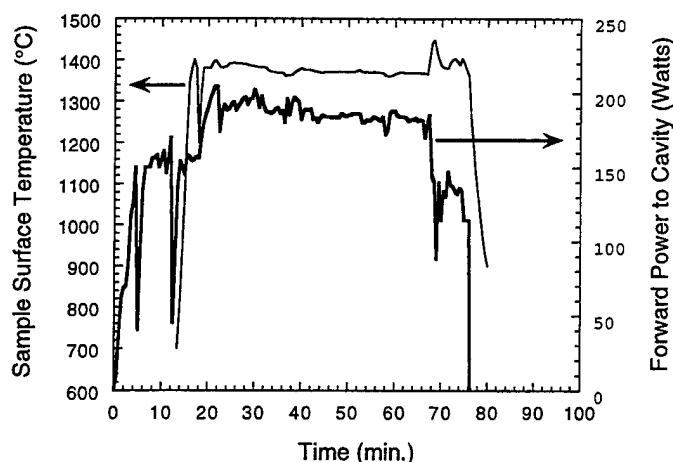
Fig. 4 – Power and temperature profiles during microwave sintering of Sample J

Table 2 – Tube Furnace Sintering Data [Initial Dens. = 57%, Initial Grain Size < 0.1 μm].

Sample	T (°C)	Hold Time (min.)	% RD	Grain Size (μm)	Hardness (GPa)
F1	1100	60	64	0.2	2.9
J1	1223	60	77	0.3	7.4
I1	1393	60	97	3.0	18.9

0.1 wt% MgO, a grain growth inhibitor, and were microwave sintered in a vacuum. As discussed above, our experiments were carried out in a nitrogen atmosphere, however, there was no indication of nitridation in the X-ray diffraction results. The LANL/Varian experiments employed an air atmosphere [19, 20]. The hold time for the ORNL compacts was 60 min, and for the LANL/Varian data, it was about 5 min. There is mixed agreement between the various data sets. There is good agreement between the ORNL and our conventionally sintered results. Our microwave data agree reasonably well with the conventionally sintered data. The short hold-time data are shifted to ~100°C higher temperatures than the conventional sintering data in the region of significant change of densification with temperature. This shift is reduced for the 60-min hold-time microwave data, suggesting that the shift toward higher temperatures is related to the shorter processing time of the microwave data. The LANL/Varian 60 GHz data are in fairly good agreement with our short hold-time data. In contrast, the ORNL microwave data show densification occurring at much lower temperatures (300 to 500°C) than the conventional sintering data and the other high-frequency microwave results.

The average grain size of the sintered compact represents a key parameter of the sintered compact as most desirable material properties scale inversely with grain size. The grain size was estimated from scanning electron micrographs (SEM). A selection of these is shown in Fig. 6, which shows the evolution of the microstructure of the AKP-50$^{\text{TM}}$ compacts from the as-pressed condition through various 35 GHz microwave sintering temperatures. The initial microstructure of the as-pressed compact, which is 55% to 60% dense, is one of aggregated particles of approximately 0.1 to 0.2 μm in size. At intermediate sintering temperatures, 1090 to 1300°C, the microstructure evolves
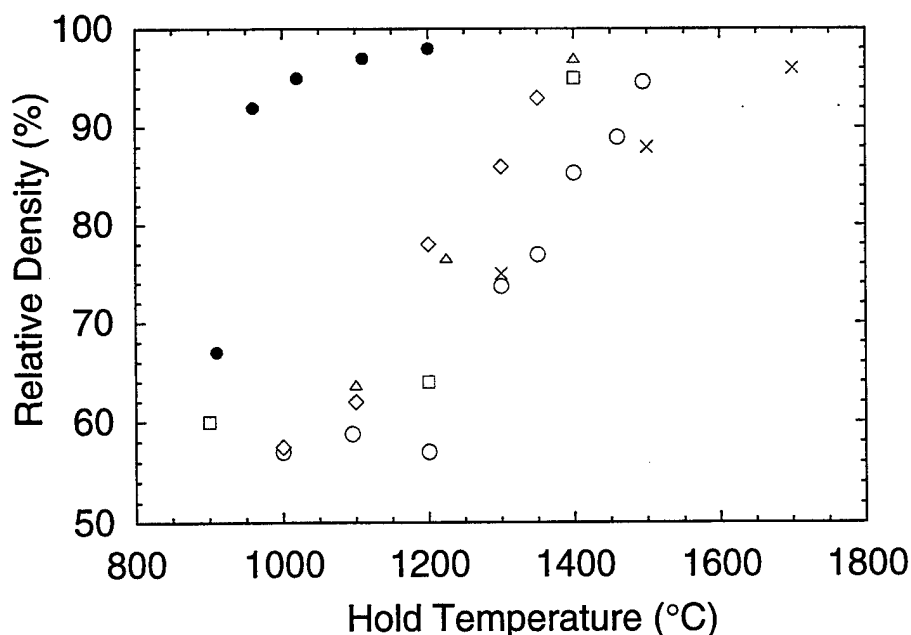
Fig. 5 – Comparison of data for densification obtained by millimeter-wave processing and conventional pressure-free sintering. o: NRL, short hold-time 35 GHz microwave sintered (MS); □: NRL, long hold-time 35 GHz MS; △: NRL, conventionally sintered (CS); •: ORNL, 28 GHz MS; ◇: ORNL, CS; and ×: LANL/Varian, 60 GHz MS.

gradually, with little obvious change notable. There is very little grain growth with the grain size, only 0.2 to 0.3 μm at a sintering temperature of 1300°C, scarcely larger than the starting particle size. There is increased evidence of interparticle sintering (neck formation and growth) over this temperature range, but the grains remain rounded without well-defined crystalline facets. There is also very little elimination of the initial intra-agglomerate porosity at this point, in agreement with the minimal changes in the compact density for this temperature range. At a sintering temperature of 1350°C, more distinct crystalline facets are evident but still with no evidence of significant grain growth. There is also evidence here of more rapid sintering, leading to elimination of intra-agglomerate porosity as large clusters of grains sinter together. At the highest sintering temperature shown in Fig. 6, 1495°C, the grains are now well crystallized with distinct crystalline facets. Grain growth remains moderate, with grain sizes ranging from 0.5 to 1.0 μm at this sintering temperature. Small residual pores are evident at the grain triple points; these are sufficient in number to account for most of the remaining porosity in the sample. There is little evidence of any impurity phases or glassy phases at the grain boundaries in this sample, confirming the high purity of the starting material. Impurities would be evidenced as thick grain-boundary regions between grains and by material left on grain boundary surfaces exposed by fracturing the sample for SEM. Glassy phases would appear similarly and would also be shown through rounding of the corners of the triple-point pores between grains. Such rounding is not evident, indicating that there is very little glassy phase present. Beyond the highest sintering temperature shown, elimination of the residual triple-point pores shown in the absence of any second phase grain growth inhibitors at the grain boundaries (ORNL used MgO for this purpose) permits more rapid grain growth with further sintering, as shown in Fig. 7, for densities above approximately 90% of the theoretical maximum.
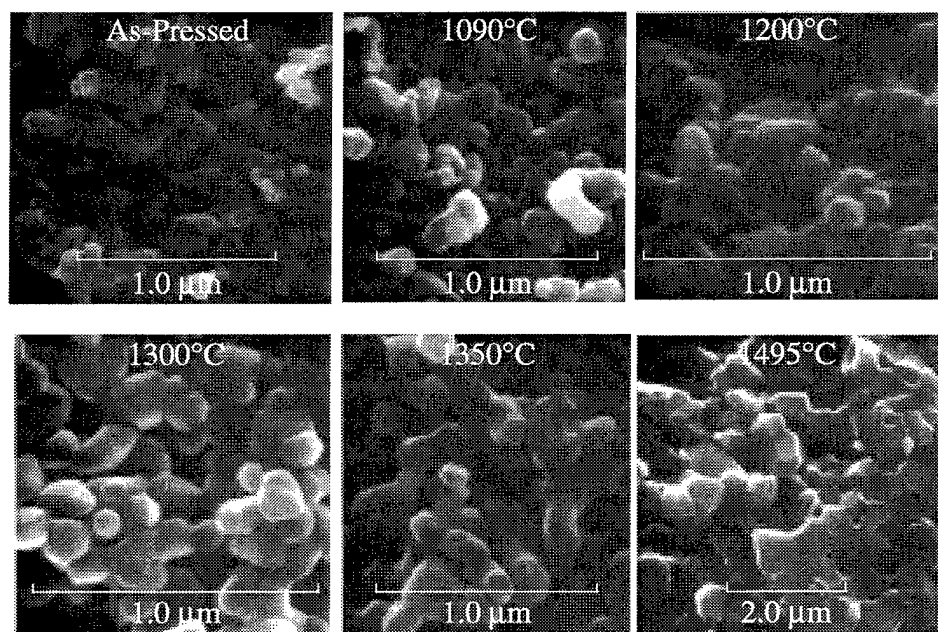
Fig. 6 – SEMs of 35-GHz microwave sintered Sumitomo AKP-50 alumina for several peak hold temperatures

The grain size data from this work and a data point from the LANL/Varian experiment are plotted as a function of relative density in Fig. 7. The figure shows a high degree of correlation between grain size and relative density (i.e., all the Sumitomo AKP-50^{TM} alumina data, both microwave and conventional, with widely different heating rates, hold times, and peak sintering temperatures lie along a single curve). This curve indicates that initial densification occurs with little grain growth until a relative density of 90% is achieved, after which the remaining densification is accompanied by rapid grain growth. This type of behavior is characteristic of a high-purity single component oxide material, where the major restraint on grain growth is the residual porosity [21]; our data indicate that it is insensitive to the heating profile and the heat source.

Figure 8 shows our hardness data, which show good agreement between the microwave and conventionally sintered Sumitomo AKP-50^{TM} as a function of relative density.

4. DISCUSSION AND CONCLUSIONS

In this work, high-purity Sumitomo AKP-50^{TM} alumina compacts have been sintered to 95% RD using a few hundred watts of 35 GHz microwave power. In spite of the rapid heating and cooling, none of the sintered compacts showed signs of cracking. A detailed comparison of microwave and conventionally sintered compacts produced from the same batch showed no significant differences in densification, grain growth, or hardness. The volumetric coupling of the microwave field to the workpiece allows more rapid heating and cooling than in a conventional furnace, significantly shortening the total processing time.

An analysis of the time-averaged microwave interaction with vacancies near a grain surface
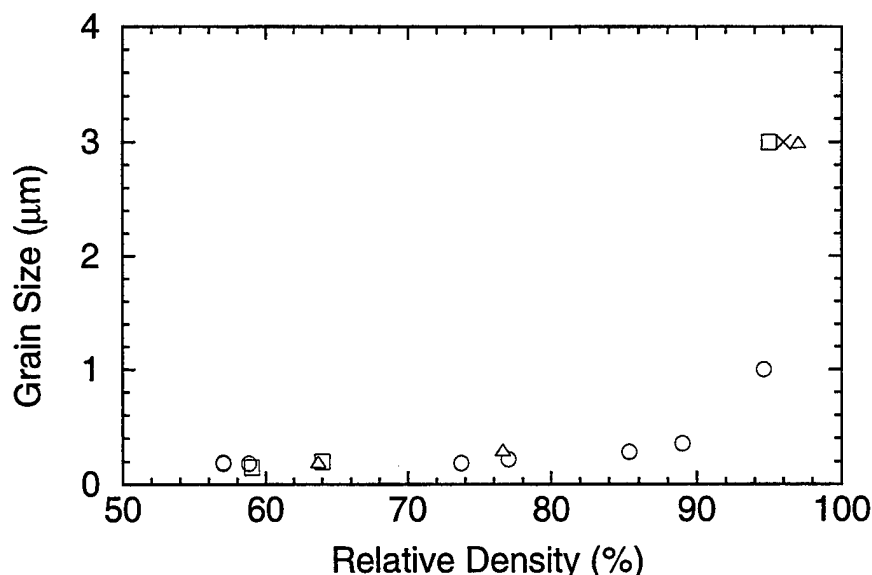
Fig. 7 – Sintered-compact grain size as a function of relative density. Same symbol definitions as in Fig. 5.

indicates that the resulting stress is much less than the pressure resulting from excess surface energy, at least in the case of alumina. Thus this type of nonthermal effect is not expected to play a role in the sintering process. This conclusion is supported by our experimental results.

Our microwave data clearly do not agree with the ORNL 28 GHz data [2], which showed densification occurring at much lower temperatures than for conventional sintering. This has implications regarding the activation enthalpy for sintering, which in Ref. 2 was calculated to be much less for 28 GHz microwave sintering of alumina than for conventional sintering. An analysis of possible errors in our temperature measurements suggests that our pyrometer data underestimate the workpiece temperature by up to a few tens of degrees. This is because we are making a surface measurement, whereas microwave heating usually produces hotter temperatures in the interior and because of radiative losses due to the pyrometer view hole. Thus errors in our temperature measurement are unlikely to account for the difference in the results. The differences in hold time are also unlikely to account for all of the difference, as sintering is roughly linear with time and exponential with temperature, and the effective hold time always includes portions of the heating and cooling cycles. Another explanation, that of different sintering atmospheres (i.e., hard vacuum in the ORNL experiments vs nitrogen in our work) should not account for the differences, as alumina is extremely difficult to reduce [22], and there is little effect of sintering atmosphere on the initial sintering rate. Reduction of alumina, via increased lattice defects, would enhance bulk diffusion, which is important only in the final stages of sintering. In the earlier stages of sintering, surface and vapor transport predominate, and these are not significantly affected by the reduction of the alumina. There is no evidence (visual, XRD, SEM) of AlON formation. Although the AKP-50™ used did not have the 0.1-wt% MgO as did the ORNL material, this also should not account for the temperature differences, as MgO is a grain-growth *inhibitor* rather than a *sintering aid* that could possibly lower the densification temperature. Finally, there was no evidence of plasma formation, at least exterior to the workpiece, during the sintering process.

In summary, the present study of the microwave sintering of a well-characterized alumina pow-
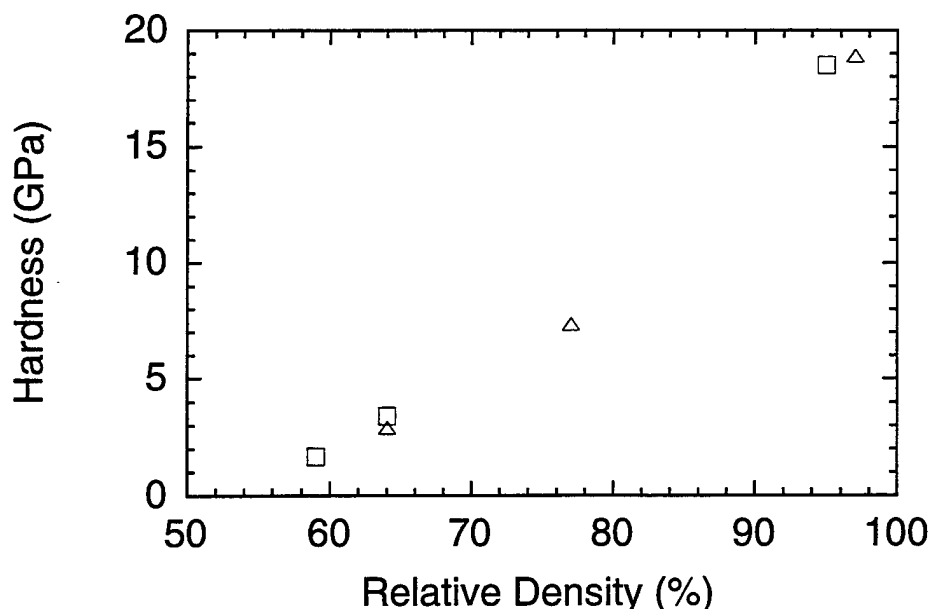
Fig. 8 – Hardness of sintered alumina as a function of relative density. Same symbol definitions as in Fig. 5.

der shows no significant differences between microwave and conventional processing, including the temperature and temperature dependence of densification, grain growth, and hardness. Note that recent microwave processing experiments on other ceramic materials continue to show differences particularly in processing time and temperature [9, 10], suggesting the possibility of other as yet unidentified factors. Obtaining accurate temperature measurements in the microwave environment, though not a factor in our work, continues to be a challenge as pointed out by Bykov et al. [11].

5. ACKNOWLEDGMENTS

REFERENCES

1. D.E. Clark, D.C. Folz, R.L. Schulz, Z. Fathi, and A.D. Cozzi, *MRS Bull.* **18**(11), 41–46 (1993).

2. M.A. Janney and H.D. Kimrey, "Microwave Sintering of Alumina at 28 GHz," in *Ceramic Powder Science II*, G.L. Messing, E.R. Fuller, and H. Hausner, eds. (American Ceramic Society, Westville, Ohio, 1988), p. 919.

3. T.T. Meek, R.D. Blake, and J.J. Petrovic, "Microwave Sintering of AL_2O_3 and Al_2O_3–SiC Whisker Composites," *Ceram. Eng. Sci. Proc.* **8**, 861 (1987).

4. J. Freim, J. McKittrick, J. Katz, and K. Sickafus, "Phase Transformation and Densification Behavior of Microwave Sintered γ-Al_2O_3," *Mat. Res. Soc. Symp. Proc.* **347**, 525 (1994).

5. Y.V. Bykov and V.E. Semenov, "Processing of Material Using Microwave Radiation," in *Applications of High-Power Microwaves*, A.V. Gaponov-Grekhov and V.L. Granatstein, eds. (Artech House, Boston, 1994), p. 319.

6. A.W. Fliflet, R.W. Bruce, A.K. Kinkead, R.P. Fischer, D. Lewis III, R. Rayne, B. Bender, L.K. Kurihara, G.-M. Chow, and P.E. Schoen, "Application of Microwave Heating to Ceramic Processing: Design and Initial Operation of a 2.45 GHz Single-Mode Furnace," *IEEE Tran. Plasma Sci.* **24**, 1041–1049 (1996).

7. D. Lewis III, R.J. Rayne, B.A. Bender, L.K. Kurihara, G-M. Chow, A. Fliflet, A. Kinkead, and R. Bruce, "Conventional and High Frequency Microwave Processing of Nanophase Ceramic Materials," *Nanostruct. Mat.* **9**, 97-100 (1997).

8. R.W. Bruce, A.W. Fliflet, R.P. Fischer, D. Lewis III, B. Bender, G.-M. Chow, R. Rayne, L.K. Kurihara, and P.E. Schoen, "Millimeter Wave Processing of Alumina Compacts," *Ceram. Trans.* **80**, 287–294 (1997).

9. G. Link, W. Bauer, A. Weddigen, H.-J. Ritzhaupt-Kleissel, and M. Thumm, "MM-Wave Processing of Ceramics," *Ceram. Trans.* **80**, 303–311 (1997).

10. S. Miyake, Y. Sethuhara, S. Kinoshita, S. Sano, M. Kamai, T. Ohmae, and N. Abe, "Study of Ceramic Heating and Sintering by High-Power Millimeter-Wave Radiation Within JWRI at Osaka University," *Ceram. Trans.* **80**, 313–320 (1997).

11. Y.V. Bykov, A.G. Eremeev, V.V. Holoptsev, "Sintering of Piezoceramics Using Millimeter-Wave Radiation," *Ceram. Trans.* **80**, 321–328 (1997).

12. K.I. Rybakov and V.E. Semenov, "Possibility of Plastic Deformation of an Ionic Crystal Due to the Nonthermal Influence of a High-Frequency Electric Field," *Phys. Rev. B* **49**, 64–68 (1994).

13. R.L. Coble and J.E. Burke, "Sintering in Ceramics," in *Progress in Ceramic Science* **3**, J.E. Burke, ed. (Macmillan, New York, 1963), Ch. 4.

14. R. Pampuch, *Constitution and Properties of Ceramic Materials*, (Elsevier, New York, 1991), Part II, Ch. 2.

15. S.A. Freeman, J.H. Booske, and R.F. Cooper, "Microwave Field Enhancement of Charge Transport in Sodium Chloride," *Phys. Rev. Lett.* **74**, 2042–2045 (1995).

16. S.A. Freeman, "Investigations of Non-Thermal Interactions Between Microwave Fields and Ionic Ceramic Materials," Ph.D. thesis, University of Wisconsin, Madison, WI, 1996.

17. I. Sakaguchi, V. Srikanth, T. Ikegami, and H. Haneda, "Grain Boundary Diffusion of Oxygen in Alumina Ceramics," *J. Amer. Ceram. Soc.* **78**, 2557–2559 (1995).

18. R. Joesten, "A Diffusion–Compensation Relation for Normal Grain Growth and Grain-Boundary Diffusion of Qxygen in Qxides," *Commun. Am. Ceram. Soc.*, C-62–C-64 (1985).

19. H. Huey, Micramics, Inc., Cupertino, CA, private communication, Jan. 1998.

20. T.T. Meek, University of Tennessee, Knoxville, TN, private communication, Jan. 1998.

21. K. Yematsu, R.M. Cannon, R.D. Bagley, M.F. Xan, U. Chowdhay, and H.K. Bowen, "Microstructure Evolution Controlled by Dopants and Pores at Grain Boundaries," Proceedings of the International Symposium of Factors in Densification and Sintering of Oxide and Non-Oxide Ceramics, 1978, Tokyo Institute of Technology, Tokyo, Japan, pp. 190–205.

22. I.S. Kulikov, "Thermodynamic Analysis of the System Al_2O_3-C," *Metall.* **6**, 55-60 (1986).

Appendix

THEORY OF MICROWAVE–VACANCY INTERACTION

In microwave sintering, thermal energy is deposited volumetrically in the workpiece by one or more loss mechanisms involving high-frequency oscillations of vacancies or other constituents of the material induced by the microwave field. The microwave field can also interact with the vacancies to produce concentration changes on a much longer time scale. This type of interaction leads to mass transport rather than to the generation of thermal energy. To investigate the possibility of significant nonthermal microwave effects under sintering conditions, we consider the interaction of a microwave field on the vacancies present in a grain of ceramic material. Our approach follows the prescription of Rybakov and Semenov [A1].

In sintering, we are ultimately concerned with grain boundary motion caused by the vacancy flux at the grain surface. The grain boundary velocity in the normal direction is given by

$$v_{nS} = -\hat{n} \cdot \vec{J}_{vS}, \tag{A1}$$

where J_v is the total vacancy flux at the surface. Assuming there are no vacancy sinks or sources in the grain interior, the concentration and flux of vacancies of type α are related by Fick's equation

$$\frac{\partial N_\alpha}{\partial t} + \vec{\nabla} \cdot \vec{J}_\alpha = 0, \tag{A2}$$

where N_α is the vacancy concentration and J_α is the vacancy flux. In the presence of an applied microwave field $\vec{\mathcal{E}}(\vec{r}, t) = \vec{\mathcal{E}}_0(\vec{r}) \cos(\omega t)$, the vacancy flux is determined by diffusion and microwave-induced drift processes and is given by

$$\vec{J}_\alpha = -D_\alpha \vec{\nabla} N_\alpha + D_\alpha N_\alpha \frac{q_\alpha \vec{E}}{k_B T}, \tag{A3}$$

where $\vec{E} = \vec{\mathcal{E}} - \vec{\nabla}\varphi$, $\vec{\nabla}\varphi$ is a slowly varying potential due to charge separation, and the Nerst-Einstein relation for mobility has been assumed. In Eq. (A3), D_α is the vacancy diffusion coefficient, q_α is the vacancy charge, k_B is the Boltzmann constant, and T is the temperature. Since the wavelength of the microwave field is much larger than the dimensions of the grain, the microwave field in the grain can be treated in the quasistatic approximation

$$\vec{\nabla} \times \vec{E} \approx 0 \tag{A4}$$

$$\vec{\nabla} \cdot \vec{E} = \frac{1}{\varepsilon_0 \varepsilon'} \sum_\alpha \frac{q_\alpha N_\alpha}{\Omega_\alpha}, \tag{A5}$$

where α is summed over the vacancy types, $\varepsilon_0 = 8.85 \times 10^{-12} \mathrm{F/m}$ is the permittivity of free space, and ε' is the real part of the normalized dielectric constant of the grain. SI (Systems International)

units are used throughout unless otherwise noted. At the grain boundary, the vacancy flux and concentration satisfy the boundary conditions

$$\hat{n} \cdot \sum_{\alpha} q_{\alpha} \vec{J}_{\alpha S} = 0 \tag{A6}$$

$$\hat{n} \cdot \sum_{\alpha} \vec{J}_{\alpha S} = \sum_{\alpha} \beta_{\alpha} (N_{\alpha S} - N_{\alpha 0 S}), \tag{A7}$$

where $\hat{n}$ is the outward unit normal at the grain surface; $J_{\alpha S}$ and $N_{\alpha S}$ are the surface flux and concentration of vacancies, $N_{\alpha 0 S}$ denotes the vacancy concentration in the absence of the microwave field; and β_{α} is a kinetic coefficient that characterizes the vacancy surface permeability. Equation (A6) stipulates that no net current flows across the grain surface, and Eq. (A7) states that the vacancy flux across the grain surface is determined by the surface permeability for vacancies. At the surface, the vacancy concentration is modified by a stress $\vec{\sigma}_s$, resulting from surface energy or an applied force, according to

$$N_{\alpha 0 S} = N_{\alpha 0} e^{\hat{n} \cdot \vec{\sigma}_s \Omega_{\alpha} k_B T}. \tag{A8}$$

Solving Eqs. (A2) to (A5) subject to the boundary conditions Eqs. (A6) and (A7) yields the vacancy concentrations and electromagnetic fields in the grain, allowing the effect of microwave fields on the mass transport during sintering to be calculated. Following Rybakov and Semenov, we use a perturbation approach that assumes that the microwave-induced changes in the vacancy distributions are small. This assumption is generally well justified. The vacancy concentration is expressed in the form:

$$N_{\alpha} = N_{\alpha 0} + \nu_{\alpha} + \nu_{\alpha}^{(2)} + \eta_{\alpha}, \tag{A9}$$

where $N_{\alpha 0}$ is the equilibrium vacancy concentration, ν_{α} and $\nu_{\alpha}^{(2)}$ are the first and second order high-frequency perturbations due to the microwave field satisfying $N_{\alpha 0} \gg |\nu_{\alpha}| \gg |\nu_{\alpha}^{(2)}|$, and η_{α} is a slow-time-scale perturbation due to the microwave field also satisfying $N_{\alpha 0} \gg |\eta_{\alpha}|$. Substituting Eqs. (A3) and (A9) into Eq. (A2) and equating high-frequency terms leads to

$$\frac{\partial \nu_{\alpha}}{\partial t} - D_{\alpha} \nabla^2 \nu_{\alpha} + \frac{D_{\alpha} N_{\alpha 0} q_{\alpha}}{\varepsilon_0 \varepsilon' k_B T} \vec{\nabla} \cdot \vec{\mathcal{E}} = 0. \tag{A10}$$

Similarly, substituting Eq. (A9) into Eq. (A5) and equating high-frequency terms leads to

$$\vec{\nabla} \cdot \vec{\mathcal{E}} = \frac{1}{\varepsilon_0 \varepsilon'} \sum_{\beta} \frac{q_{\beta} \nu_{\beta}}{\Omega_{\beta}}, \tag{A11}$$

where β here denotes the vacancy type. Finally, substituting Eq. (A11) into Eq. (A10) leads to

$$\frac{\partial \nu_{\alpha}}{\partial t} - D_{\alpha} \nabla^2 \nu_{\alpha} + \frac{D_{\alpha} N_{\alpha 0} q_{\alpha}}{\varepsilon_0 \varepsilon' k_B T} \sum_{\beta} \frac{q_{\beta} \nu_{\beta}}{\Omega_{\beta}} = 0. \tag{A12}$$

Next, we consider a one-dimensional (1–D) solution in the near-surface region and assume the high-frequency vacancy perturbations have the form $\nu = \text{Re} \{\hat{\nu}(x) e^{i\omega t}\}$, where x denotes the coordinate in the direction normal to the grain surface. Substituting this expression into Eq. (A12) leads to

$$i\omega \hat{\nu}_{\alpha} - D_{\alpha} \frac{d^2 \hat{\nu}_{\alpha}}{dx^2} + \frac{D_{\alpha} N_{\alpha 0} q_{\alpha}}{\varepsilon_0 \varepsilon' k_B T} \sum_{\beta} \frac{q_{\beta} \hat{\nu}_{\beta}}{\Omega_{\beta}} = 0. \tag{A13}$$

Averaging the vacancy flux given by Eq. (A3) over a wave period, the quasistationary flux is found to be

$$\vec{j}_\alpha = \left\langle \vec{J}_\alpha \right\rangle = -\frac{D_\alpha}{k_B T} \vec{\nabla} \mu_\alpha + \frac{D_\alpha q_\alpha}{k_B T} \left\langle \nu_\alpha \vec{\mathcal{E}} \right\rangle, \tag{A14}$$

where

$$\mu_\alpha = k_B T \eta_\alpha + q_\alpha N_{\alpha 0} \varphi, \tag{A15}$$

and Fick's equation for the quasistatic flux becomes (we assume $\partial \eta_\alpha / \partial t \ll \vec{\nabla} \cdot \vec{j}_\alpha$)

$$\vec{\nabla} \cdot \vec{j}_\alpha \approx 0. \tag{A16}$$

Time-averaging the surface boundary conditions, Eqs. (A6) and (A7), over a wave period leads to

$$\hat{n} \cdot \sum_\alpha q_\alpha \vec{j}_{\alpha S} = 0 \tag{A17}$$

$$\hat{n} \cdot \sum_\alpha \vec{j}_{\alpha S} = \sum_\alpha \beta_\alpha \left(\frac{\mu_{\alpha S}}{k_B T} - \frac{N_{\alpha 0} \sigma_s \Omega_\alpha}{k_B T} \right), \tag{A18}$$

where $\beta_\alpha = \langle \beta_\alpha \rangle$ has been assumed, and Eq. (A8) has been used with the approximation $e^{\hat{n} \cdot \vec{\sigma}_s \Omega_\alpha k_B T} \approx 1 + \hat{n} \cdot \vec{\sigma}_s \Omega_\alpha k_B T$.

As pointed out by Rybakov and Semenov and shown below, the high-frequency vacancy perturbations are localized in a thin near-surface layer, the thickness of which scales as the characteristic diffusion length $\ell_c = \sqrt{D/\omega}$. Since within the near-surface layer the vacancy flux is essentially constant as shown by Eq. (A17), Eq. (A14) can be rewritten as

$$\frac{D_\alpha}{k_B T} \vec{\nabla} \mu_\alpha + \vec{j}_\alpha' = \frac{D_\alpha q_\alpha}{k_B T} \left\langle \nu_\alpha \vec{\mathcal{E}} \right\rangle, \tag{A19}$$

where the " $'$ " denotes a quantity in the bulk region. In the bulk region, the vacancy flux satisfies

$$\vec{j}_\alpha' = -\frac{D_\alpha}{k_B T} \vec{\nabla} \mu_\alpha'. \tag{A20}$$

Substituting Eq. (A20) into Eq. (A19) leads to

$$\vec{\nabla} \left(\mu_\alpha - \mu_\alpha' \right) = q_\alpha \left\langle \nu_\alpha \vec{\mathcal{E}} \right\rangle. \tag{A21}$$

Taking the normal component of Eq. (A21) and integrating yields

$$\mu_\alpha \approx \mu_\alpha' + \int q_\alpha \left\langle \nu_\alpha \hat{n} \cdot \vec{\mathcal{E}} \right\rangle dx. \tag{A22}$$

Substituting Eq. (A22) into Eq. (A18) leads to

$$\sum_\alpha \left(\hat{n} \cdot \vec{j}_{\alpha S} - \frac{\beta_\alpha \mu_{\alpha S}'}{k_B T} \right) = \sum_\alpha \beta_\alpha \left(\frac{1}{k_B T} \int_{-\infty}^0 q_\alpha \left\langle \nu_\alpha \hat{n} \cdot \vec{\mathcal{E}} \right\rangle dx - \frac{N_{\alpha 0} \hat{n} \cdot \vec{\sigma}_s \Omega_\alpha}{k_B T} \right). \tag{A23}$$

At this point, it is convenient to limit the analysis to a single type of vacancy or two oppositely charged but otherwise identical vacancies and introduce the microwave-induced vacancy pressure

$$p = \int_{-\infty}^0 \sum_\alpha \frac{q_\alpha}{\Omega_\alpha} \left\langle \nu_\alpha \hat{n} \cdot \vec{\mathcal{E}} \right\rangle dx. \tag{A24}$$

Substituting Eq. (A11) into Eq. (A24) and using the 1–D form of the vacancy concentration perturbation enables the microwave pressure to be rewritten as

$$p = \frac{\varepsilon_0 \varepsilon'}{2} \left(\left\langle \hat{n} \cdot \vec{\mathcal{E}}(0)^2 \right\rangle - \left\langle \hat{n} \cdot \vec{\mathcal{E}}(-\infty)^2 \right\rangle \right). \tag{A25}$$

Making use of Eq. (A24), approximating the gradient of μ'_α as $\nabla \mu'_\alpha \approx \mu'_\alpha / R$ where R is the grain radius, and making use of Eqs. (A16) and (A20), Eq. (A23) can be rewritten as:

$$\sum_\alpha \hat{n} \cdot \vec{j}_\alpha S = \left(1 - \frac{\beta_v R}{D_v} \right)^{-1} \frac{\beta_v N_0 \Omega_v}{k_B T} \left(\frac{p}{N_0} - \hat{n} \cdot \vec{\sigma}_s \right). \tag{A26}$$

Using Eq. (A1) leads to an expression for the dimensionless grain deformation rate (defined as $\dot{\varepsilon} = v_S / 2R$)

$$\dot{\varepsilon} = - \left(1 - \frac{\beta_v R}{D_v} \right)^{-1} \frac{\beta_v N_0 \Omega_v}{2 R k_B T} \left(\frac{p}{N_0} - \hat{n} \cdot \vec{\sigma}_s \right). \tag{A27}$$

Finally, if the kinetic coefficient is assumed to satisfy $\beta_v \gg D_v / R$, Eq. (A27) simplifies to

$$\dot{\varepsilon} \approx \frac{D_v N_0 \Omega_v}{2 R^2 k_B T} \left(\frac{p}{N_0} - \hat{n} \cdot \vec{\sigma}_s \right). \tag{A28}$$

If the microwave pressure is identified with a compressive stress given by

$$\sigma_E = \frac{p}{N_0}, \tag{A29}$$

then Eq. (A28) has the same form as the equation for the pressure-free sintering deformation rate corresponding to volume diffusion [A2]. Thus the nonthermal microwave interaction results in an enhanced volume diffusion sintering deformation rate

$$\dot{\varepsilon} \approx \frac{D_v N_{v0} \Omega_v}{2 R^2 k_B T} \left(\sigma_E + \sigma^s \right). \tag{A30}$$

Clearly, the importance of this enhancement depends on the magnitude of the stress σ_E.

Single Vacancy Species

We begin the investigation of solutions of Eq. (A13) by considering the case of a ceramic with only one type of vacancy present. Then Eq. (A13) reduces to a second-order ordinary differential equation with constant coefficients of the form:

$$\frac{d^2 \hat{\nu}}{dx^2} - k^2 \hat{\nu} = 0, \tag{A31}$$

where

$$k^2 = i \frac{\omega}{D} + \frac{q^2 N_0}{\varepsilon_0 \varepsilon' \Omega k_B T}. \tag{A32}$$

The solution is of the form:

$$\hat{\nu} = A e^{kx} + B e^{-kx}, \tag{A33}$$

where k can be expressed as

$$k = \sqrt{\frac{i \omega \varepsilon}{\varepsilon' D}}. \tag{A34}$$

The complex dielectric constant ε is given by

$$\varepsilon = \varepsilon' - i\varepsilon_v'', \tag{A35}$$

where

$$\varepsilon_v'' = \frac{\sigma_v}{\varepsilon_0 \omega} \tag{A36}$$

and $\sigma_v = DN_0 q^2 / \Omega k_B T$ is the conductivity associated with vacancy diffusion. Assuming $\varepsilon_v'' \ll \varepsilon_v'$,

$$k \approx \sqrt{\frac{i\omega}{D}} = \sqrt{\frac{\omega}{D}} \frac{1+i}{\sqrt{2}}. \tag{A37}$$

In this approximation the high-frequency concentration perturbation is of the form

$$\nu = \mathrm{Re}\left\{ \nu_0 e^{\frac{(1+i)}{\sqrt{2}\ell_c}x + i\omega t} \right\}, \tag{A38}$$

where $\ell_c = \sqrt{D/\omega}$.

To obtain the normal component of the perturbed high-frequency field, Eq. (A38) is substituted into Eq. (A11). Canceling time-dependent factors leads to, using the notation $\mathcal{E}_n = \hat{n} \cdot \vec{\mathcal{E}}$ and $\mathcal{E}_n(t) = \mathrm{Re}\left\{ \hat{\mathcal{E}}_n e^{i\omega t} \right\}$,

$$\frac{d\hat{\mathcal{E}}_n}{dx} = \frac{q\nu_0}{\varepsilon_0 \varepsilon' \Omega} e^{\frac{1+i}{\sqrt{2}\ell_c}x}. \tag{A39}$$

Integrating Eq. (A39) from $-\infty$ to x yields

$$\hat{\mathcal{E}}_n(x) = \hat{\mathcal{E}}_n(-\infty) + \frac{q\nu_0 \ell_c (1-i)}{\sqrt{2}\varepsilon_0 \varepsilon' \Omega} e^{\frac{1+i}{\sqrt{2}\ell_c}x}. \tag{A40}$$

To find ν_0, substitute Eq. (A9) into the surface boundary condition Eq. (A7) and keep terms up to first order in the perturbation expansion. Then Eq. (A7) can be written as

$$-D\frac{d\nu}{dx} - D\frac{d\eta}{dx} + \frac{DqN_0 \mathcal{E}_n S}{k_B T} = \beta\nu + \beta\eta - \frac{\beta N_0 \sigma_s \Omega}{k_B T}. \tag{A41}$$

Collecting high-frequency terms and using Eq. (A38) leads to

$$\left(\frac{D(1+i)}{\sqrt{2}\ell_c} - \beta \right)\nu_0 + \frac{DqN_0 \mathcal{E}_n S}{k_B T} = 0. \tag{A42}$$

Next, assuming the microwave frequency is high enough that $\sqrt{D\omega} \gg \beta$, the second term on the left-hand side of Eq. (A42), associated with vacancy fluxes through the grain surface, can be neglected and, using Eq. (A40) with $\mathcal{E}_{nS} = \mathcal{E}_n(0)$, the following expression is obtained:

$$\nu_0 = \frac{\sqrt{2}qN_0 \ell_c}{k_B T(1+i)} \hat{\mathcal{E}}_n(-\infty). \tag{A43}$$

Substituting Eq. (A43) into Eq. (A40) leads to

$$\hat{\mathcal{E}}_n(-\infty) = \frac{\hat{\mathcal{E}}_n(0)}{1 - i\sigma_v/\varepsilon_0 \varepsilon' \omega}. \tag{A44}$$

Finally, substituting Eq. (A44) into Eq. (A25), expanding the denominator and retaining lowest order terms leads to an expression for the microwave pressure in the high-frequency limit:

$$p = \frac{1}{4\varepsilon_0 \varepsilon'} \left(\frac{\sigma_v}{\omega} \right)^2 |\mathcal{E}_n(0)|^2. \tag{A45}$$

Oppositely Charged Vacancy Species

Consider a ceramic material with two types of vacancies that are oppositely charged but otherwise identical. Then Eq. (A13) can be expressed as a pair of coupled, inhomogeneous second-order ordinary differential equations with constant coefficients of the form:

$$\frac{d^2\hat{\nu}_1}{dx^2} - k^2\hat{\nu}_1 = -\frac{\hat{\nu}_2}{\lambda^2} \tag{A46}$$

$$\frac{d^2\hat{\nu}_2}{dx^2} - k^2\hat{\nu}_2 = -\frac{\hat{\nu}_1}{\lambda^2}, \tag{A47}$$

where

$$\frac{1}{\lambda^2} = \frac{q^2 N_0}{\varepsilon_0 \varepsilon' \Omega k_B T}. \tag{A48}$$

Approximate solutions to these coupled equations can be obtained by an iterative method. In the lowest order approximation, Eqs. (A46) and (A47) become

$$\left(\frac{d^2}{dx^2} - k^2\right)\hat{\nu}_1^{(1)} = -\frac{\hat{\nu}_2^{(0)}}{\lambda^2} \tag{A49}$$

$$\left(\frac{d^2}{dx^2} - k^2\right)\hat{\nu}_2^{(1)} = -\frac{\hat{\nu}_1^{(0)}}{\lambda^2}, \tag{A50}$$

where $\hat{\nu}_{1,2}^{(0)}$ are solutions of the homogeneous equation

$$\left(\frac{d^2}{dx^2} - k^2\right)\hat{\nu}_{1,2}^{(0)} = 0. \tag{A51}$$

It can be shown that the solutions for the region $x < 0$ are of the form [A3]:

$$\hat{\nu}_1^{(1)} = +\nu_{10}\left(1 + \frac{kx}{2\left(1 + i\lambda^2/\ell_c^2\right)}\right)e^{kx} \tag{A52}$$

$$\hat{\nu}_2^{(1)} = -\nu_{10}\left(1 + \frac{kx}{2\left(1 + i\lambda^2/\ell_c^2\right)}\right)e^{kx}. \tag{A53}$$

Following the prescription used in the single vacancy case, one finds

$$\hat{\mathcal{E}}(x) = \hat{\mathcal{E}}(-\infty) + \frac{2q\nu_{10}}{\varepsilon_0\varepsilon'\Omega k}\left(1 + \frac{kx - 1}{2\left(1 + i\lambda^2/\ell_c^2\right)}\right)e^{kx} \tag{A54}$$

and

$$\nu_{10} = \frac{1}{\left(k^2 + \frac{1}{4k^2\lambda^4}\right)}\frac{kqN_0}{k_B T}\hat{\mathcal{E}}_n(-\infty). \tag{A55}$$

Substituting these expressions into Eq. (A25), one finds that the microwave pressure for two vacancies in the high-frequency limit is increased by a factor of four compared to the single vacancy case, i.e.,

$$p^{(2v)} = \frac{1}{\varepsilon_0\varepsilon'}\left(\frac{\sigma_v}{\omega}\right)^2|\mathcal{E}_n(0)|^2. \tag{A56}$$

REFERENCES

A1. K.I. Rybakov and V.E. Semenov, "Possibility of Plastic Deformation of an Ionic Crystal Due to the Nonthermal Influence of a High-Frequency Electric Field," *Phys. Rev. B***49**, 64–68 (1994).

A2. R. Pampuch, *Constitution and Properties of Ceramic Materials* (Elsevier, New York, 1991), Part II, Ch. 2.

A3. E.A. Coddington, *An Introduction to Ordinary Differential Equations* (Prentice-Hall, Englewood Cliffs, N.J., 1961), Ch. 2.